Exploring monovalent copper compounds with oxygen and hydrogen

Pavel A. Korzhavyi[a,1], Inna L. Soroka[b], Eyvaz I. Isaev[c,d,2], Christina Lilja[e], and Börje Johansson[a,f]

[a]Departments of Materials Science and Engineering, and [b]Applied Physical Chemistry, Royal Institute of Technology, SE-100 44 Stockholm, Sweden; [c]Department of Physics, Chemistry, and Biology, Linköping University, SE-581 83 Linköping, Sweden; [d]Department of Theoretical Physics, National University of Science and Technology "Moscow Institute of Steel and Alloys," Moscow 119049, Russia; [e]Swedish Nuclear Fuel and Waste Management Company, Box 250, SE-101 24 Stockholm, Sweden; and [f]Materials Theory, Department of Physics and Astronomy, Uppsala University, Box 516, SE-751 20 Uppsala, Sweden

Edited* by Ho-Kwang Mao, Carnegie Institution of Washington, Washington, DC, and approved November 17, 2011 (received for review September 27, 2011)

New important applications of copper metal, e.g., in the areas of hydrogen production, fuel cell operation, and spent nuclear fuel disposal, require accurate knowledge of the physical and chemical properties of stable and metastable copper compounds. Among the copper(I) compounds with oxygen and hydrogen, cuprous oxide Cu_2O is the only one stable and the best studied. Other such compounds are less known (CuH) or totally unknown (CuOH) due to their instability relative to the oxide. Here we combine quantum-mechanical calculations with experimental studies to search for possible compounds of monovalent copper. Cuprous hydride (CuH) and cuprous hydroxide (CuOH) are proved to exist in solid form. We establish the chemical and physical properties of these compounds, thereby filling the existing gaps in our understanding of hydrogen- and oxygen-related phenomena in Cu metal.

electronic structure | lattice dynamics | thermodynamic properties | metastability | infrared spectra

Copper in compounds may exist in oxidation states ranging from +1 to +4, although the +2 (cupric) and +1 (cuprous) are the most common ionic states of copper (1). At ambient conditions, the most stable compounds of copper with oxygen and hydrogen are copper(II) oxide CuO (stable) and copper(II) hydroxide $Cu(OH)_2$ (metastable) (1, 2). Among the compounds of monovalent copper with oxygen and hydrogen, cuprous oxide Cu_2O is known to be the only stable and therefore best-studied compound (1–5). Cu_2O has the cuprite crystal structure (Fig. 1*A*), in which the copper(I) cations, Cu^+, are arranged into a face-centered cubic (fcc) sublattice and the oxygen anions, O^{2-}, reside on the sites of a body-centered cubic (bcc) sublattice (6). Each O^{2-} is tetrahedrally coordinated by Cu^+, whereas the coordination of Cu^+ ions is linear (7).

The equilibrium solubility of hydrogen in fcc Cu is very low, and there is no stable hydride in the CuH binary system (8, 9). However, a metastable copper hydride CuH with the hexagonal ZnS (wurtzite) structure (10) can be formed chemically (11) or electrochemically (12, 13). Although CuH is the oldest metal hydride known (synthesized by Wurtz in 1844) (11), there have been very few experimental (10–16) and practically no theoretical (see, however, ref. 17) studies of CuH. Copper(I) hydride decomposes readily into Cu and H_2 (gas) in vacuum or ambient air, as well as under electron or laser beam. Similar to other metal hydrides, copper(I) hydride is pyrophoric, but unlike them, it is not water reactive. Therefore, CuH may safely be kept in water at a T of approximately 0 °C or in an inert gas atmosphere at a T of approximately −50 °C (13–16).

Cuprous hydroxide CuOH has not been proven to exist in a solid form, and its properties are completely unknown. Experimental information on thermodynamic properties is available only for charge-neutral molecular CuOH species in aqueous solution (2). The formation of submonolayer of adsorbed OH species on Cu surfaces has been reported recently (18, 19).

In the present work, we apply first-principles calculations to search for (meta-) stable Cu–O–H compounds and to compute their electronic and phonon spectra. Such compounds are then synthesized using wet-chemical methods and characterized by nondestructive experimental techniques. The details of theoretical and experimental procedures used in this study are given in the *SI Text*.

Results and Discussion

Electronic and Phonon Spectra Calculations. Our search for locally stable configurations of Cu^+, O^{2-}, H^-, and/or H^+ ionic species was performed using electronic structure calculations based on density-functional perturbation theory (20, 21), taking into account the contribution from lattice vibrations to the thermodynamic properties (22). Initial configurations were based on the close-packed (fcc and hexagonal) sublattice of Cu^+ ions and, alternatively, on the bcc sublattice of O^{2-} ions. The study yielded solid-state configurations and phonon spectra of cuprous oxide Cu_2O, cuprous hydride CuH, and cuprous hydroxide CuOH (Fig. 1 *A*–*C*). Their local stability is consistent with the calculated semiconducting electronic structure (Fig. S1) that is indicative of saturated chemical bonding in each of these compounds.

The phonon spectra of the three compounds contain (*i*) low-frequency peaks (below 200 cm^{-1}), which are due to the acoustic and optical phonon modes that involve motion of the relatively heavy Cu^+ ions, and (*ii*) high-frequency peaks (above 400 cm^{-1}), which are due to the optical modes associated with vibrations of lightweight species (O^{2-} and/or $H^{+/-}$). Thus, a group of peaks (band) situated at 500–650 cm^{-1} in the phonon spectrum of Cu_2O (Fig. 1*A* and Fig. S2) corresponds to the vibrations of O^{2-} inside a tetrahedron formed by the four neighboring Cu^+ ions in the cuprite structure. The spectrum of copper hydride CuH (Fig. 1*B* and Fig. S3) has a high-frequency band lying between 900 and 1,140 cm^{-1} that corresponds to the optical vibrations of a hydride ion, H^-, surrounded by a tetrahedron of Cu^+ cations. The large difference in mass between the ^{63}Cu and ^1H isotopes creates a wide gap between the corresponding optical modes in the phonon spectrum of CuH. The high-frequency part of the CuOH spectrum (Fig. 1*C* and Fig. S4) is represented by two peaks situated around 500 cm^{-1} (and associated with the optical vibrations involving motion of a hydroxyl OH^- group as a whole), a band at about 900 cm^{-1} (Cu–O–H bond bending mode, associated with changing the angle between the Cu–O and O–H bonds), and a high-frequency band at about 3,400 cm^{-1} (O–H bond stretching mode).

Author contributions: P.A.K., C.L., and B.J. designed research; P.A.K., I.L.S., and E.I.I. performed research; E.I.I. contributed new reagents/analytic tools; P.A.K., C.L., and B.J. analyzed data; and P.A.K. and I.L.S. wrote the paper.

The authors declare no conflict of interest.

*This Direct Submission article had a prearranged editor.

[1]To whom correspondence should be addressed. E-mail: pavel@mse.kth.se.

[2]Deceased September 11, 2011.

This article contains supporting information online at www.pnas.org/lookup/suppl/doi:10.1073/pnas.1115834109/-/DCSupplemental.

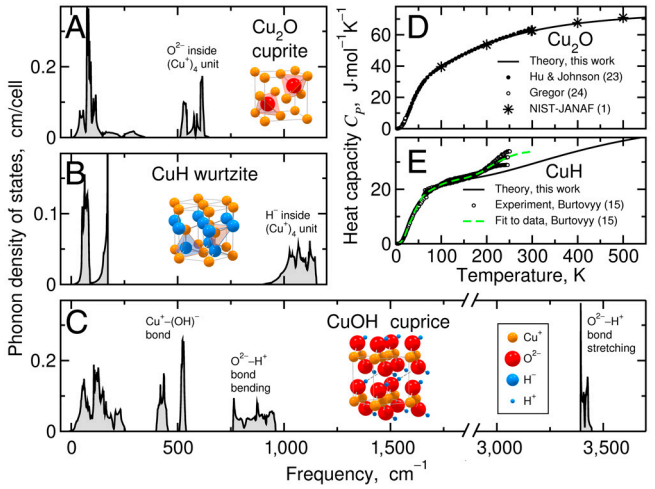

Fig. 1. Phonon spectra and heat capacity of copper(I) compounds. (*A*–*C*) Phonon density of states of (*A*) cuprite Cu_2O calculated at the lattice parameter $a = 4.27$ Å, (*B*) wurtzite CuH calculated at the lattice parameters $a = 2.904$ Å, and (*C*) CuOH, calculated at molecular volume of 30.7 Å^3. (*D* and *E*) Calculated and experimental (1, 15, 23, 24) heat capacities C_P, of Cu_2O (*D*), and CuH (*E*). Note that the break in the experimental specific heat curve (*E*) at about 60 K is due to differences in the specimens' composition and cooling techniques used above and below that temperature (15).

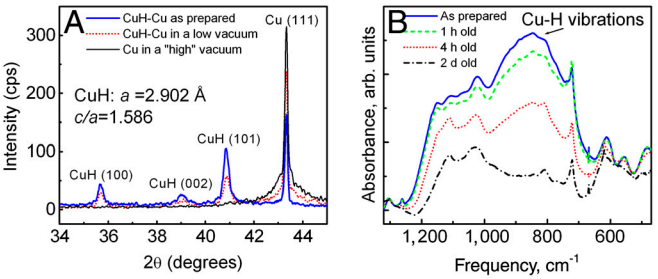

Fig. 2. Experimental results for copper hydride. (*A*) X-ray diffraction patterns obtained for as-prepared CuH at ambient pressure (blue thick line) and for the same sample at pressures of 10^{-3} torr (red dotted line) and 10^{-5} torr (black line) (*B*) FTIR spectra of CuH. The spectra were recorded from one sample at different moments of time: as-prepared CuH (solid blue line), after 1 h (dashed green line), after 4 h (dotted red line), and after 2 d (dot-dashed black line) of exposure to air at room temperature.

The presence of a wide gap in the phonon spectra of these compounds, between the low- and high-frequency bands, should be reflected in the temperature dependence of heat capacity. The calculated heat-capacity (C_P) curves for Cu_2O and CuH are shown in Fig. 1 *D* and *E* (see also Fig. S5) in comparison with experimental data from previous calorimetric studies (1, 15, 23, 24). As seen from the figure, the shapes of C_P curves for cuprous oxide (for temperatures below 500 K) and cuprous hydride (below 170 K) are accurately accounted for by the present calculations that employ the quasi-harmonic approximation. Also, these calculations qualitatively reproduce the negative thermal expansion anomaly of cuprous oxide at low temperatures (see Fig. S6 and refs. 22 and 25). The experimental curves for CuH exhibit an additional, broad peak feature at about 200 K, which is unexpected from the calculated phonon spectra. The position and the height of this peak feature appear to depend on the hydrogen content of the specimens (15). The amount of excess entropy associated with this peculiarity suggests that, depending on the hydrogen substoichiometry of CuH_x ($x < 1$), the H^- ions become mobile at temperatures around 200 K, so that the hydrogen sublattice "melts," while the copper sublattice remains solid. Thus, one may interpret the C_P anomaly in copper(I) hydride as a signature of a superionic transition. This interpretation is supported by the rapid evolution of hydrogen gas from the sample (Fig. S7) and by the large values of root-mean-square atomic displacements, exceeding 0.5 Å, calculated for hydrogen ions in CuH (Fig. S8). Because of the large amplitude, the hydrogen motion in CuH requires theoretical techniques going beyond the quasi-harmonic approximation employed in the present study. However, our conclusion about the strong anharmonic effects in CuH qualitatively accounts for the larger width of the absorption band, found in our infrared spectroscopy measurements at about 900 cm^{-1} (Fig. 2*B*), as compared to the calculated width of the H^- peak in the phonon spectrum of CuH (Fig. 1*B*).

Experimental Studies of CuH. The copper hydride powder has been synthesized by the wet-chemical method described in ref. 13. The structural and optical properties of CuH have been studied using X-ray diffraction (XRD) analysis and FTIR spectroscopy, respectively.

The XRD patterns (Fig. 2*A*) were recorded from the same CuH sample in three subsequent runs. The first pattern was recorded from the as-prepared sample at atmospheric pressure; the next two records were made after lowering the pressure to 10^{-3} and 10^{-5} torr, respectively. The as-prepared sample consisted of a mixture of CuH and Cu crystallites; no other reflections were found within the explored 2θ range from 20° to 120°. The XRD pattern from the as-prepared sample is consistent with the hexagonal wurtzite structure of CuH having the lattice parameters $a = b = 2.902$ and $c = 4.602$ Å. The measured lattice parameters are very close (within 1%) to those reported in the literature (10, 13) as well as to our theoretical values (Table 1).

Using the data of Fig. 2*A*, one can follow the dynamics of the CuH decomposition in vacuum. The diffraction peaks of CuH rapidly lose their intensity with lowering the external pressure and merge with the background at a pressure of about 10^{-5} torr. At the same time, the intensity of the diffraction peaks from metallic copper increases. As seen from the figure, the Cu(111) diffraction peak from the specimen labeled as "high vacuum" consists of two overlapping peaks having the same position but very different widths, which corresponds to a bimodal size distribution of the Cu particles. From the peak widths, the diameters for the two main fractions of Cu particles are calculated to be about 15 and 160 nm, respectively, where the finer fraction has formed by the decomposition of CuH.

Further XRD studies of CuH specimens, exposed to air at atmospheric pressure and room temperature for varying periods of time, revealed that the CuH decomposition into Cu metal and H_2 gas occurred gradually, much slower than in vacuum. Traces of copper hydride could be found in the sample even after 2 d of exposure to open air. Oxidation of the Cu particles formed as a result of CuH decomposition in air has been detected by the present XRD measurements, but is viewed as a secondary and minor process.

The crystallographic parameters of CuH and Cu_2O structures obtained in this work both experimentally and theoretically are listed in Table 1. Complementary to experimental results of the present and previous crystallographic studies of CuH, our calculations allowed us to determine the value of parameter z (equilibrium position of hydrogen relative to copper) in the wurtzite structure.

FTIR absorption spectra (Fig. 2*B*) have been recorded from an as-prepared CuH specimen as well as from the same specimen exposed to air for different periods of time. A prominent feature in these spectra is a broad peak, located in the frequency band from 720 to 1,180 cm^{-1}, which may be ascribed to vibrations of H^- inside the Cu^+ tetrahedron. The peak intensity decreases with time and falls down to the background level after 2 d of exposure. The FTIR spectra also contain weak absorption peaks in the range 480–610 cm^{-1}, which may be ascribed to O^{2-} and/or

Table 1. Crystallographic data for Cu_2O, CuH, and CuOH

Formula	Space group	Lattice parameters, Å		Ion	Pos.	Atomic positions		
		Calc. (this work)	Exp. (this work)			*x*	*y*	*z*
Cu_2O	$Pn\bar{3}m$, No. 224	$a = 4.30$	$a = 4.27$	O^{2-}	2a	0	0	0
	cubic			Cu^+	4b	1/4	1/4	1/4
CuH	$P6_3mc$, No. 186	$a = 2.90$	$a = 2.90$	Cu^+	2b	1/3	2/3	0
	hexagonal	$c = 4.62$	$c = 4.60$	H^-	2b	1/3	2/3	0.381
CuOH	*Cm*2*a*, No. 39	$a = 5.71$		Cu^+	4a	0	0.000	0
	orthorhombic	$b = 5.32$		O^{2-}	4c	1/4	−0.007	0.293
		$c = 4.21$		H^+	4c	1/4	0.148	0.423

H_2O impurities in the hydride. The absolute intensity of these spectral peaks is much lower than the intensity of the peak due to H^- vibrations in the as-prepared sample.

The FTIR results for the as-prepared CuH sample are in good agreement with our phonon spectrum calculations that predict the existence of an absorption band at 900–1,140 cm^{-1} and ascribe it to H^- vibrations (Fig. 1*B*). A greater width of the band is found experimentally, which can be explained by strong anharmonic effects due to the large vibration amplitudes and the diffusive mobility of hydrogen ions in CuH at room temperature.

CuOH in a Solid Form. As the crystal structure of cuprous hydroxide has not been established experimentally, it needs to be solved theoretically. The stoichiometry of CuOH dictates the formal oxidation states of the ions to be O^{2-}, Cu^+, and H^+. Our calculations reveal strong preference of Cu^+ and H^+ cations to keep the same coordination in the CuOH structure as they have in the respective oxides, Cu_2O and H_2O. There is a crystallographic relationship between the structures of Cu_2O (cuprite) and H_2O (ice). The chemical similarity between these two substances (both are monovalent oxides) becomes clearer if one considers a high-pressure phase (26) of H_2O known as ice X, which has the same cuprite structure as Cu_2O. With lowering pressure, ice X undergoes a proton-disordering transformation into ice VII (or VIII), by shifting each proton away from the bond-center position toward one of the two neighboring O^{2-} ions, to form a molecular crystal comprised of H_2O molecules connected to each other by hydrogen bonds (27). A similar asymmetric position has been obtained in recent ab initio calculations for a hydrogen impurity inside a copper vacancy in Cu_2O (28).

A variety of ionic configurations of bulk cuprous hydroxide may be derived by assembling CuOH molecules into structures which are intermediate between cuprite Cu_2O and ice VII H_2O. Two of such configurations are depicted in Fig. 3. The crystallographic parameters for the lowest-energy solid-state configuration of cuprous hydroxide CuOH (configuration 2 in Fig. 3*B*) are listed in Table 1 (bond lengths and angles are given in Table S1). Its crystal structure has been identified as orthorhombic, space group *Cm*2*a*. Both configurations shown in Fig. 3 are based on the bcc sublattice of oxygen anions (similar to cuprite). In both structures, the Cu^+ and H^+ ions are situated approximately on the line connecting the two neighboring anions. However, whereas the copper cations reside midway between the oxygen ions (again like in cuprite), the protons are shifted away from the midpoints closer to one of the two neighboring anions, thereby exhibiting the same kind of proton disorder that is present in low-pressure phases of ice. To mark this structural relationship of CuOH to both cuprite and ice, let us refer to all the so-derived configurations of bulk CuOH as "cuprice." Another reason for introducing this unifying notation is that all such configurations are nearly degenerate in energy. For example, the difference in energy between the two manifestly dissimilar configurations shown in Fig. 3 *A* and *B* is just a fraction of kilojoule per mole. Because of this near degeneracy, the real crystal structure of CuOH may be a random mixture of various possible configurations rather than just one of them.

The question of thermodynamic stability of CuOH is of importance for the analysis of corrosion behavior of copper metal (2, 29). According to our calculations (22) (see Table S2), these CuOH structures are metastable and, in the absence of oxygen, should readily decompose into the stable substances according to the reaction

$$2CuOH \rightarrow Cu_2O + H_2O. \quad [1]$$

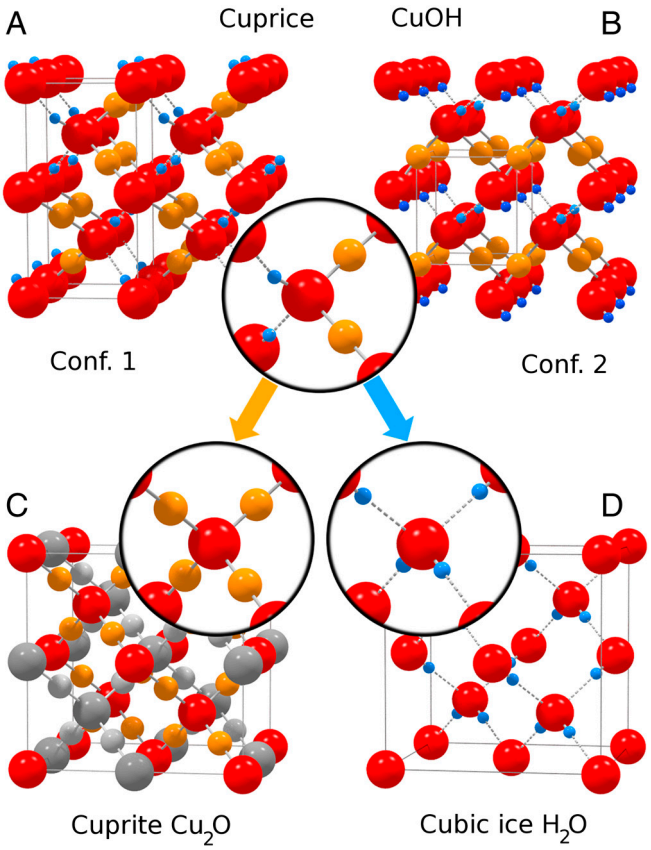

Fig. 3. The structure of CuOH and its structural relationship to those of Cu_2O and H_2O. (*A* and *B*) Two stable configurations of CuOH based on a distorted body-centered cubic sublattice of oxygen anions (similar to that in Cu_2O). Shown are just two possible variants of the spatial arrangements of Cu^+ and H^+ ions that keep the same coordination of the anions: Each O^{2-} ion in CuOH has two Cu^+ neighbors, one proton (H^+) at a short distance and one proton further away. Coordination of the cations is linear; Cu^+ ions are situated midway between the two anions, like in Cu_2O (*C*), whereas each proton is shifted away from the midpoint closer to one of the two O^{2-} neighbors but remains connected to the other O^{2-} ion by a hydrogen bond (broken line), thus facilitating the same kind of proton disorder that is present in H_2O ice (*D*). (*C*) Crystal structure of Cu_2O shown as consisting of two identical chemically disconnected (interpenetrating) anti-cristobalite lattices (one shown as colorless and the other in full color). (*D*) Cubic polymorph of ice, I_c, that has the same (apart from the proton disorder) anti-cristobalite structure as the two Cu_2O lattices (*C*).

The calculated enthalpy of this reaction is $\Delta H(298.15) = -46.1$ kJ/mol, and the Gibbs free energy is $\Delta G(298.15) = -56.4$ kJ/mol. Thus, the reaction is strongly shifted toward the formation of cuprous oxide and water, which means, in particular, that copper(I) hydroxide cannot be a stable product of copper corrosion by pure water.

Conclusions

The structural and chemical stability of copper(I) compounds with oxygen and hydrogen have been studied theoretically and experimentally. Metastable solid forms of copper(I) hydride and copper(I) hydroxide have been found and characterized. Copper (I) hydride decomposes spontaneously into metallic copper and hydrogen gas, whereas copper(I) hydroxide is theoretically predicted to decompose into cuprous oxide and water. Our experimental and theoretical results regarding the structure and properties of Cu_2O, CuH, and CuOH will be an appropriate starting point for further studies of these compounds. For instance, transient products of copper corrosion can be identified using the electronic and vibration spectra of Cu–O–H compounds obtained in this work.

Materials and Methods

First-Principles Calculations. The present electronic structure calculations are based on density-functional perturbation theory (20) and employ Vanderbilt ultrasoft pseudopotentials (30), the generalized gradient approximation (GGA) (31), and the Quantum Espresso software package (21). Total energies obtained from the electronic structure calculations have been complemented by the energy of zero-point motion of the nuclei at $T = 0$ K. Zero-point energy scales as $M^{-1/2}$, where M is the nuclear mass, and cannot be neglected for lightweight atoms such as hydrogen and oxygen. To evaluate the thermodynamic properties at finite temperatures, the calculated phonon spectra of the studied phases and of Cu metal have been integrated using the quasi-harmonic approximation (20, 32). The calculated reference energies of O_2 and H_2 molecules were corrected for the GGA atomization energy error and then combined with tabulated heat-capacity data (1) to evaluate the thermodynamic properties of the gases at finite temperatures.

X-Ray Diffraction. X-ray diffraction patterns of CuH were recorded with a Siemens D5000 diffractometer (CuK_α radiation with a wavelength $\lambda = 1.54$ Å) using Bragg–Brentano geometry. The measurements were done at room temperature and in ambient atmosphere.

FTIR. The spectra were recorded on Perkin Elmer Spectrum One FR-IR Spectrometer. The powder sample mixed with nujol was sandwiched between two plates of potassium bromide (KBr). The spectrometer was operated from 350 to 4,000 cm^{-1} at ambient temperature and atmosphere. The background correction was made using a reference KBr plate.

ACKNOWLEDGMENTS. We thank L. O. Werme, C. Ambrosch-Draxl, D. A. Andersson, O. Peil, and A. V. Ruban for fruitful discussions. I.L.S. thanks M. Ottosson for the help with XRD measurements. The work has been supported by SKB, the Swedish Nuclear Fuel and Waste Management Company.

1. Chase MW (1998) *NIST-JANAF Thermochemical Tables* (Am Inst of Physics, New York), Part II Cr-Zr, 4th Ed.
2. Puigdomenech I, Taxén C (2000) Thermodynamics data for copper: Implifications for the corrosion of copper under repository conditions. *Technical Report TR-00-13* (Swedish Nuclear Fuel Waste Manag Co, Stockholm).
3. Pourbaix M (1963) *Atlas of Electrochemical Equilibria at 25 °C (Translated from French)* (Gauthier-Villars, Paris).
4. Mattsson E (1980) Corrosion of copper and brass: Practical experience in relation to basic data. *Brit Corros J* 15:6–13.
5. Beverskog B, Puigdomenech I (1997) Revised Pourbaix diagrams for copper at 25 to 300 °C. *J Elecrochem Soc* 144:3476–3483.
6. Kirfel A, Eichhorn K (1990) Accurate structure analysis with synchrotron radiation. The electron density in Al_2O_3 and Cu_2O. *Acta Crystallogr A* 46:271–284.
7. Schäfer W, Kirfel A (2002) Neutron powder diffraction study of the thermal expansion of cuprite. *Appl Phys A Mater Sci Process* 74:s1010–s1012.
8. Predel B (1994) CuH (copper-hydrogen). *Springer Materials—The Landolt-Börnstein Database*, ed O Madelung, http://www.springermaterials.com; 10.1007/10086090_1077.
9. Verbetsky VN, Mitrokhin SV (2000) Copper- silver- and gold-hydrogen. *Solid State Phenom* 73–75:503–517.
10. Goedkoop JA, Andersen AF (1955) The crystal structure of copper hydride. *Acta Crystallogr* 8:118–119.
11. Wurtz A (1844) On copper hydride (Translated from French). *Cr Hebd Acad Sci* 18:702–704.
12. Fitzsimons NP, Jones W, Herley PJ (1992) Aspects of the synthesis of copper hydride and supported copper hydride. *Catal Letters* 15:83–94.
13. Fitzsimons NP, Jones W, Herley PJ (1995) Studies of copper hydride: Part 1. Synthesis and solid-state stability. *J Chem Soc Faraday Trans* 91:713–718.
14. Burtovyy R, Utzig E, Tkacz M (2000) Studies of the thermal decomposition of copper hydride. *Thermochim Acta* 363:157–163.
15. Burtovyy R, Włosewicz D, Czopnik A, Tkacz M (2003) Heat capacity of copper hydride. *Thermochim Acta* 400:121–129.
16. Herley PJ, Fitzsimons NP, Jones W (1995) Studies of copper hydride: Part 2. Transmission electron microscopy. *J Chem Soc Faraday Trans* 91:719–724.
17. Smithson H, et al. (2002) First-principle study of the stability and electronic structure of metal hydrides. *Phys Rev B Condens Matter Mater Phys* 66:144107.
18. Protopopoff E, Markus P (2005) Potential—pH diagrams for hydroxyl and hydrogen adsorbed on a copper surface. *Electrochim Acta* 51:408–417.
19. Forster M, et al. (2011) $c(2\times2)$ Water-hydroxyl layer on Cu(110): A wetting layer stabilized by bjerrum defects. *Phys Rev Lett* 106:046103.
20. Baroni S, de Gironcoli S, Dal Corso A, Giannozzi P (2001) Phonons and related crystal properties from density-functional perturbation theory. *Rev Mod Phys* 73:515–562.
21. Giannozzi P, et al. (2009) Quantum Espresso: a modular and open-source software project for quantum simulations of materials. *J Phys Condens Matter* 21:395502.
22. Korzhavyi PA, Johansson B (2010) Thermodynamic properties of copper compounds with oxygen and hydrogen from first principles. *Technical Report TR-10-30* (Swedish Nuclear Fuel Waste Manag Co, Stockholm).
23. Hu J-H, Johnston HL (1951) Low temperature heat capacities of inorganic solids. IX. Heat capacity and thermodynamic properties of cuprous oxide from 14 to 300 °K. *J Am Chem Soc* 73:4550–4551.
24. Gregor LV (1962) The heat capacity of cuprous oxide from 2.8 to 21 °K. *J Phys Chem* 66:1645–1647.
25. Bohnen K-P, Heid R, Pintschovius L, Soon A, Stampfl C (2009) Ab initio lattice dynamics and thermal expansion of Cu_2O. *Phys Rev B Condens Matter Mater Phys* 80:134304.
26. Hemley RJ, et al. (1987) Static compression of H_2O-ice to 128 GPa (1.28 Mbar). *Nature* 330:737–740.
27. Kamb B, Davis BL (1964) Ice VII the densest form of ice. *Proc Natl Acad Sci USA* 52:1433–1439.
28. Scanlon DO, Watson GW (2011) Uncovering the complex behavior of hydrogen in Cu_2O. *Phys Rev Lett* 106:186403.
29. King F, Padovani C (2011) Review of the corrosion performance of selected canister materials for disposal of HLW and/or spent fuel. *Corros Eng Sci Technol* 46:82–90.
30. Vanderbilt D (1990) Soft self-consistent pseudopotentials in a generalized eigenvalue formalism. *Phys Rev B Condens Matter Mater Phys* 41:7892–7895.
31. Perdew JP, Burke K, Ernzerhof M (1996) Generalized gradient approximation made simple. *Phys Rev Lett* 77:3865–3868.
32. Baroni S, Giannozzi P, Isaev EI (2010) Density-functional perturbation theory for quasi-harmonic calculations. *Rev Mineral Geochem* 71:39–57.